ACS APPLIED MATERIALS & INTERFACES

Research Article

www.acsami.org

# An Organic Coprecipitation Route to Synthesize High Voltage $LiNi_{0.5}Mn_{1.5}O_4$

Jijun Feng,*[,†,‡] Zhipeng Huang,[†] Chao Guo,[†] Natasha A. Chernova,[‡] Shailesh Upreti,[‡,§] and M. Stanley Whittingham*[,‡]

[†]Key Laboratory of Chemical Sensing & Analysis in Universities of Shandong, School of Chemistry and Chemical Engineering, University of Jinan, Jinan 250022, China

[‡]Institute for Materials Research, State University of New York at Binghamton, Binghamton, New York 13902, United States

[§]Primet Precision Materials Inc., Ithaca, New York 14850, United States

Supporting Information

**ABSTRACT:** High-voltage cathode material $LiNi_{0.5}Mn_{1.5}O_4$ has been prepared with a novel organic coprecipitation route. The as-prepared sample was compared with samples produced through traditional solid state method and hydroxide coprecipitation method. The morphology was observed by scanning electron microscopy, and the spinel structures were characterized by X-ray diffraction and Fourier transform infrared spectroscopy. Besides the ordered/disordered distribution of Ni/Mn on octahedral sites, the confusion between Li and transition metal is pointed out to be another important factor responsible for the corresponding performance, which is worthy further investigation. Galvanostatic cycles, cyclic voltammetry, and electrochemical impedance spectroscopy are employed to characterize the electrochemical properties. The organic coprecipitation route produced sample shows superior rate capability and stable structure during cycling.

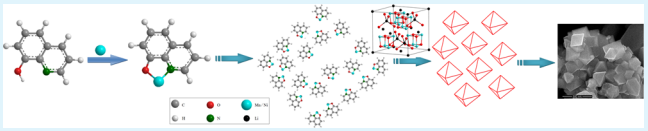

**KEYWORDS:** *organic coprecipitation, cathode material, spinel, $LiNi_{0.5}Mn_{1.5}O_4$, high voltage*

## 1. INTRODUCTION

Lithium ion batteries (LIB) have been developed successfully and widely used in the past decades. Facing the current challenge of worldwide energy shortage and ever-increasing environment pollution, LIB are expected to play crucial roles as large-scale electrical storage devices implemented in electric vehicles and modern electrical grids with intermittent renewable energy. In this context, superior cathode materials providing either higher capacity or higher voltage are in urgent demand to fulfill the requirement for enhanced energy/power density.[1−5] As a promising cathode material, spinel $LiNi_{0.5}Mn_{1.5}O_4$ has received extensive attention for its high operating voltage (4.7 V vs Li) and comparative electrochemical performance.

$LiNi_{0.5}Mn_{1.5}O_4$ is a derivative from spinel $LiMn_2O_4$. In order to improve the cycling behavior, various efforts have been focused on substitution of other metals for Mn to make $LiM_xMn_{2-x}O_4$ (M = Co, Cr, Ni, Fe, Al, Cu, etc.).[6−9] However, cycle life improved at the expense of capacity decreasing in 4.1 V plateau with an increase of the amount of doped metal. In 1995, Sigala et al.[10] found that much of the reduced capacity of Cr doped spinel $LiCr_yMn_{2-y}O_4$ materials appears in 4.9 V plateau. Soon after, the groups of Amine[11] and Dahn[12,13] reported $LiNi_{0.5}Mn_{1.5}O_4$ with one dominant plateau at around 4.7 V. Such high operating voltage not only advances energy density but also benefits the practical utilization of anode materials which have better safety but relatively higher voltage such as spinel $Li_4Ti_5O_{12}$. Batteries using $LiNi_{0.5}Mn_{1.5}O_4$ as positive electrode coupled with $Li_4Ti_5O_{12}$ as negative electrode provide high thermal stability while presenting a still feasible voltage.[14−16]

One of the main issues with this high voltage material is the unclear correlation between electrochemical performance and occupations of Ni, Mn, and even Li in the crystal lattice. Besides that, the formation of undesirable impurities during synthesis, such as NiO or $Li_xNi_{1-x}O$, is another problem. The presence of impurities deteriorates the electrochemical performance of $LiNi_{0.5}Mn_{1.5}O_4$ material. Many methods have been used to synthesize $LiNi_{0.5}Mn_{1.5}O_4$, such as solid state method,[17] sol-gel method,[18] polymer precursor method,[19,20] and microwave-assisted method.[21] It is obvious that different synthesis procedures have strong influences on the morphology, structure, and electrochemical performance of as-prepared materials.[22−25]

Coprecipitation has been generally accepted to be an appropriate method to prepare materials based on solid solution or mixed-metal oxides. In most cases, some kinds of inorganic precipitant were employed to obtain carbonate or hydroxide precipitation followed by filtering and repeated washing to get rid of the residual $OH^-$ and/or $CO_3^{2-}$. Apart from the lower yield aroused by solution loss, a noteworthy problem is the structure defects in final samples resulted from

Received: July 23, 2013
Accepted: September 27, 2013
Published: September 27, 2013

  

**Scheme 1. Schematic Illustration of 8-Hydroxyquinoline Coprecipitation Route**

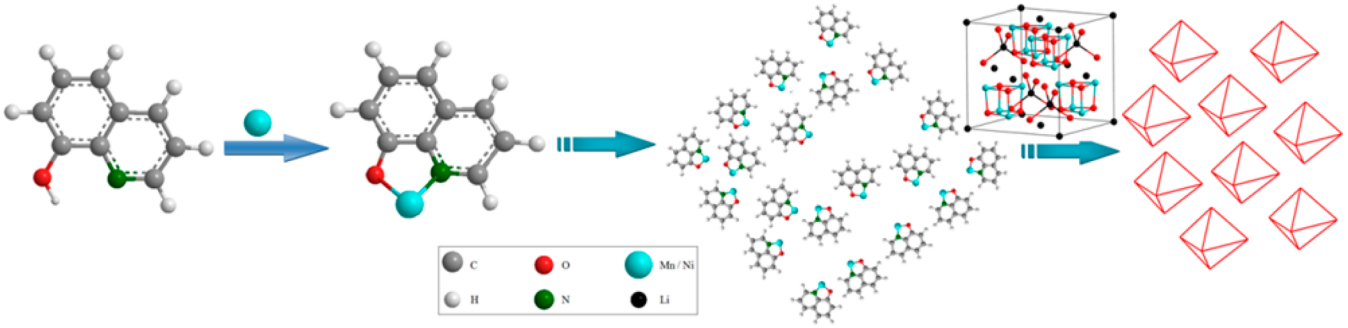


nonstoichiometric loss of different metal ions during washing procedure.[26] In this work, a novel organic precipitant, 8-hydroxyquinoline, was used to get the coprecipitation precursor. Since the organic precipitator can be easily removed during the high temperature calcination process, the precipitation washing step can be omitted. Moreover, Li was added in the solution accompanied with Ni and Mn accurately and settled in the precipitation simultaneously, avoiding the deviation introduced when calculating the amount of Li compounds according to the weight of precipitation precursors in case of the oxidation of some $Ni^{2+}$ during drying.

## 2. EXPERIMENTAL SECTION

The stoichiometrical $Ni(Ac)_2{\cdot}6H_2O$, $Mn(Ac)_2{\cdot}4H_2O$, and LiAc were dissolved in deionized water (solution A) at ambient temperature, and 8-hydroxyquinoline was dissolved in ethanol at 60°C (solution B). The solution A was added to solution B dropwise with constant stirring to get brown flocculent precipitation. The solid−liquid dispersion was vigorously stirred for 2 h followed by evaporation of solvent at 80°C without filtration. After drying in air at 100°C, the precipitation was preheated at 470°C for 5 h to get a dark power precursor. The precursor was pressed into pellets at 15 MPa and subsequently sintered in air at 800°C for 24 h with heating rate of 10°C/min and cooling rate of 1°C/min. The as-prepared sample was marked as QC. To compare, samples were prepared using solid-state method (marked as SS) and normal coprecipitation method with KOH as precipitant (marked as HC) as well. All the samples were subjected to a calcination procedure at 800°C for 24 h in air.

X-ray diffraction (XRD) was performed on a Scintag XDS2000 $\theta$-$\theta$ diffractometer equipped with Cu Ka radiation and a Ge (Li) solid state detector. The data were recorded during step scan in the $2\theta$ range of 10−90°, with step size and exposure time set as 0.02° and 8 s separately. The Rietveld refinement was done with GSAS/EXPGUI package.[27,28] Morphology of the samples was observed on a FEI QUANTA FEG 250 scanning electron microscope (SEM). Fourier transform infrared (FTIR) spectroscopy was conducted with a Thermo Nicolet Nexus 670 FT-IR spectrometer with a spectral resolution of 4 $cm^{-1}$.

Electrochemical experiments were operated on Biologic VMP multichannel potentiostats with CR2325 coin cells. For fabrication of cathode electrodes, 80 wt % as-prepared materials were mixed with 10 wt % carbon black and 10 wt % polyvinylidene fluoride (PVDF) in *N*-methylpyrrolidinone (NMP). The slurry thus obtained was cast onto aluminum foil and then dried at 90°C overnight in vacuum. The coin cells were assembled in a helium-filled glove box with lithium metal pellets as negative electrodes, 1 M $LiPF_6$ in EC+DEC (1:1 volume ratio) as electrolytes and Celgard 2300 membrane as separators.[29] The galvanostatic cycle tests were operated between the potential limits of 3.2 and 4.9 V (vs $Li/Li^+$) with diverse rate current. At least three testing coin cells were assembled simultaneously for every sample, and the representative ones were chosen to compare. Cyclic voltammetry (CV) was recorded in a potential range from 3.2 to 4.9 V at a scanning rate of 0.05 mV $s^{-1}$. Electrochemical impedance spectroscopy (EIS) was collected in the frequency range of 200 kHz to 5 mHz with an ac amplitude of 5 mV.

## 3. RESULTS AND DISCUSSION

Organic precipitation has been used in gravimetric analysis and industry wastewater treatment with superior effects to conventional hydroxide precipitation. To our knowledge, it has not been reported to prepare cathode materials. The precipitation process is illustrated in Scheme 1. $Ni^{2+}$ and $Mn^{2+}$ can be easily combined with 8-hydroxyquinoline through the rigid O, N-bidentated chelating ligands. This could be beneficial in a more complete precipitation process, more precisely stoichiometric product and higher productivity.

The SEM images of samples obtained from different synthesis methods are shown in Figure 1. The solid state

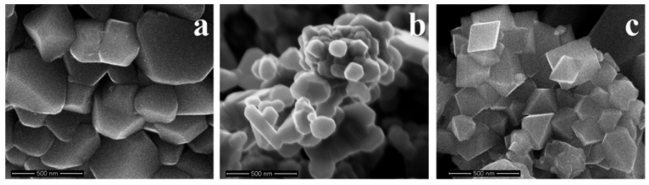


**Figure 1.** SEM images of (a) samples SS, (b) samples HC, and (c) samples QC.

method produced sample SS shows polyhedral shapes in Figure 1a with a wide particle size distribution, which is typical for materials synthesized by the solid state method. The hydroxide coprecipitation method produced sample HC, as shown in Figure 1b, consists of irregular polygon sheets with first particle size around 100 nm. The morphology of organic coprecipitation route produced $LiNi_{0.5}Mn_{1.5}O_4$ power takes on aggregation of well-shaped octahedral quasi-single crystal with an average first particle size of about 150 nm. The surface facets of the octahedrons correspond to (111) crystal planes which are thermodynamically more stable.[30]

The XRD pattern of the sample QC is shown in Figure 2 together with patterns of HC and SS for comparison. Referring to the standard card (JCPDS: 80-2184) as shown in the bottom of Figure 2a, all the three samples can be identified as cubic structures corresponding to the spinel $LiNi_{0.5}Mn_{1.5}O_4$. No superstructure peaks reflecting the ordered Ni/Mn distribution on octahedral sites were discernible, maybe because of the weak intensity. It is generally admitted that the high temperature calcination results in oxygen deficient and formation of $Li_xNi_{1-x}O$ impurities. This also happened to all the three samples as denoted by arrows in Figure 2b. However, it is obvious that the peaks attributed to $Li_xNi_{1-x}O$ impurities

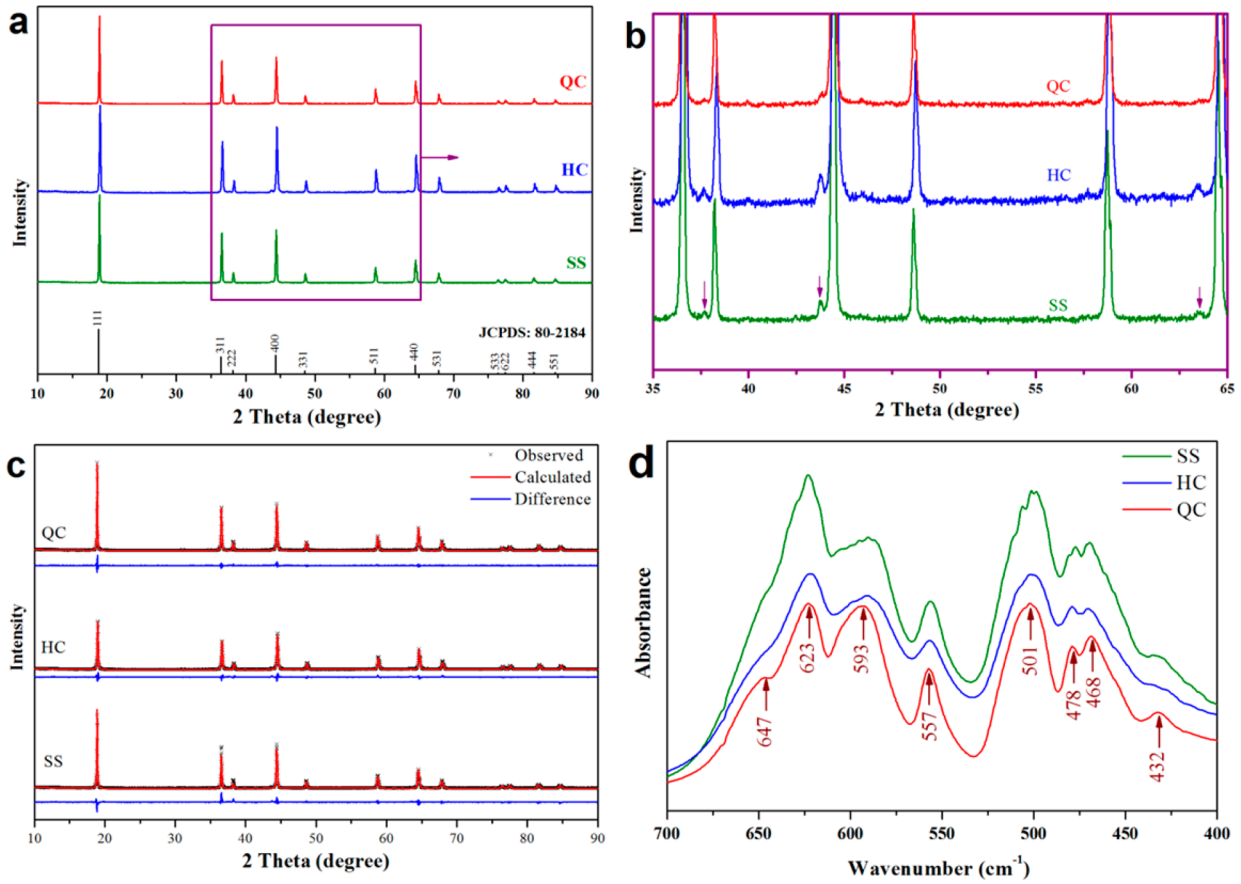


**Figure 2.** Structure of $LiNi_{0.5}Mn_{1.5}O_4$. (a) XRD patterns of samples QC, HC, and SS; (b) enlarged pattern of the box part in (a); (c) XRD Rietveld refinement of samples QC, HC, and SS; (d) FTIR spectra of samples QC, HC, and SS.

**Table 1. Comparison of Peak Intensity and Refinement Results of XRD**

| | relative intensity | | | intensity ratio | | refinement results | | |
|---|---|---|---|---|---|---|---|---|
| sample | $I_{111}$ | $I_{311}$ | $I_{400}$ | $I_{111}/I_{311}$ | $I_{311}/I_{400}$ | $a$/Å | $V$/Å$^3$ | $Rp$/% |
| SS | 100 | 56.4 | 60.0 | 1.773 | 0.940 | 8.188 | 548.995 | 6.34 |
| HC | 100 | 58.6 | 75.0 | 1.706 | 0.781 | 8.171 | 545.602 | 6.35 |
| QC | 100 | 49.0 | 53.1 | 2.041 | 0.923 | 8.174 | 546.112 | 5.76 |
| JCPDS (80-2184) | 100 | 38.2 | 42.6 | 2.618 | 0.897 | 8.170 | 545.339 | |

present much lower intensity, even hardly discernible, in the pattern of sample QC than the other ones. This indicates that the organic precipitation route can prevent the formation of $Li_xNi_{1-x}O$ impurities and oxygen deficient to a great extent, owing to the even mixing and strictly stoichiometric precursor.

Although most reports suggest that the disordered $LiNi_{0.5}Mn_{1.5}O_4$ shows superior cycle performance and rate capability to the ordered one, it is still a subject of debate. Much attention has been focused on the dependence between ordered/disordered distribution of Ni/Mn ions on the octahedral sites and the electrochemical performance.[31] However, it has been rarely aware of that the confusion between lithium ions and transition metal ions would also be responsible for the corresponding electrochemical performance of this high-voltage cathode material. For spinel structure, the (111) diffraction peak is the strongest line, while the (311) diffraction peak is the strongest line for antispinel structure with location switching of A/B atoms in $AB_2O_4$ formula. Thus, the intensity ratio $I_{111}/I_{311}$ is an important implication for the extent of confusion between lithium ions and transition metal ions in spinel $LiNi_{0.5}Mn_{1.5}O_4$. As listed in Table 1, the $I_{111}/I_{311}$ ratio of organic precipitation method produced sample QC is 2.041, which is evidently higher than that of the other two samples and much closer to that of standard JCPDS data. The lower confusion results in the smooth path for Li transport; therefore, advanced rate capability is highly expected.

It is well known for spinel $LMn_2O_4$ that the intensity ratio $I_{311}/I_{400}$ reflects the degree of tetragonal distortion from cubic spinel structure.[32] Therefore, the $I_{311}/I_{400}$ ratio could also reflect structure integrity of the $LiNi_{0.5}Mn_{1.5}O_4$ spinel structure. As listed in Table 1, sample SS and sample QC have higher $I_{311}/I_{400}$ value, while sample HC presents a lower value than that of JCPDS (80-2184) card. Among the three samples, sample QC has the less deflection from the standard JCPDS (80-2184) data. The differences of $I_{311}/I_{400}$ ratio may have something to do with $Mn^{3+}$. To further understand that, XRD data were refined, as shown in Figure 2c, and the calculated lattice parameters are summarized in Table 1. It is noticeable that all the three samples have larger unit cell than the standard $P4_332$ structure. Among them, sample SS possesses much larger


dx.doi.org/10.1021/am4029526 | ACS Appl. Mater. Interfaces 2013, 5, 10227−10232

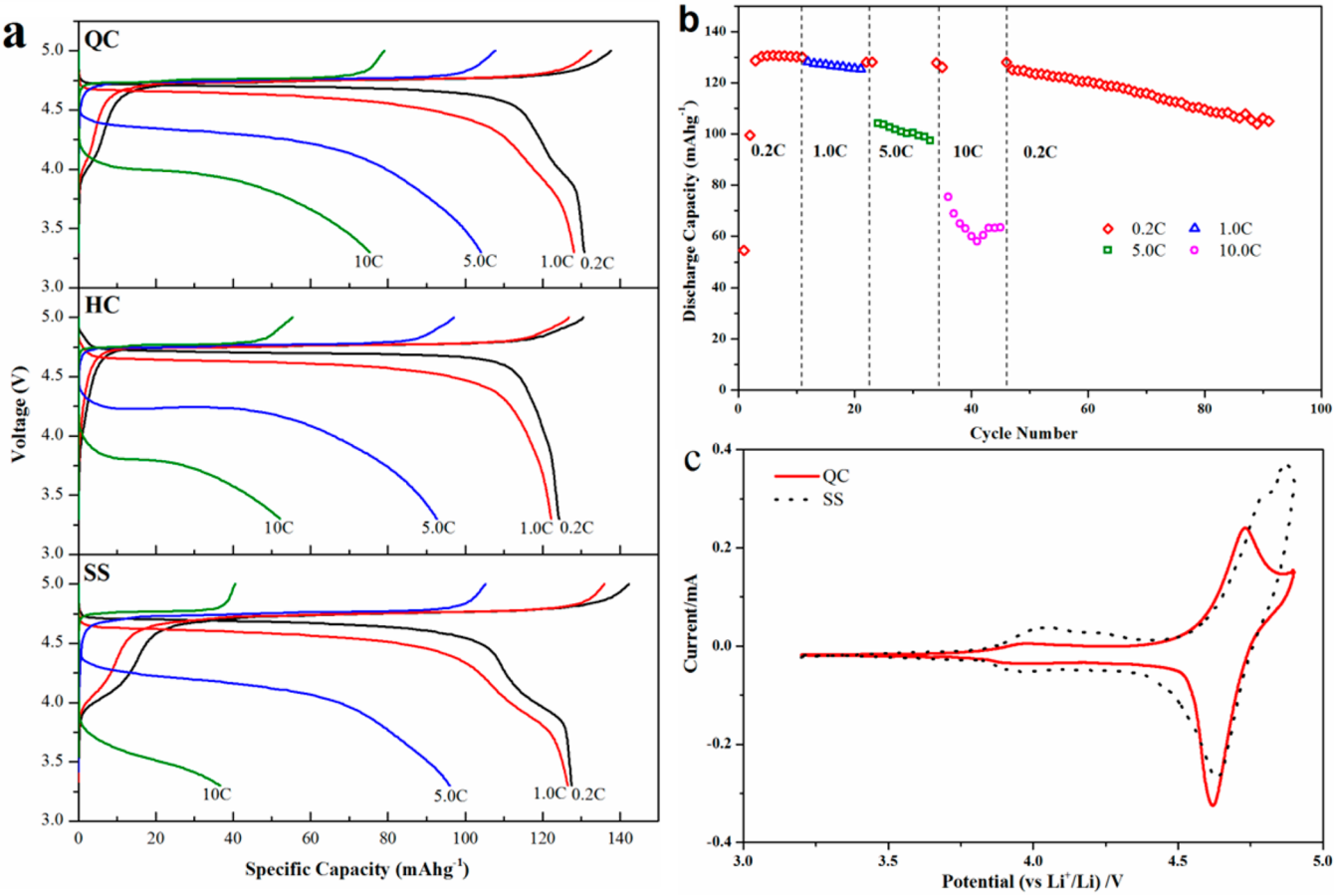


**Figure 3.** Electrochemical performance of $LiNi_{0.5}Mn_{1.5}O_4$ (a) charge curves and discharge curves at 0.2C, 1.0C, 5.0C, and 10C rates; (b) cycle performance of sample QC; (c) CV curves.

unit size, while sample HC has the smallest one. This should be attributed to the presence of $Mn^{3+}$. The lattice parameters increase with the increase in the amount of $Mn^{3+}$, since the ionic radius of $Mn^{3+}$ (0.65 Å) is larger than that of $Mn^{4+}$ (0.54 Å).[33] This is coherent with the result of discharge profiles as discussed later.

Although there should be some extra peaks in the XRD patterns of ordered $P4_332$ simple cubic structure, it's still not sufficient to distinguish ordered/disordered structure because of the low intensity of these superstructure peaks. FTIR spectroscopy has been proven to be an effective technique to differentiate the ordered and disordered structures of the nickel−manganese spinel.[34] The samples with ordered cation occupancy exhibit a series of fingerprint bands at 432, 468, 478, 501, 557, 593, 623, and 647 $cm^{-1}$.[35] On the other hand, the broadening profile and the absence of such characteristic bands, especially the shoulder peaks at 647 and 432 $cm^{-1}$ and the double bands at 468 and 478 $cm^{-1}$, indicate the disordered cation occupancy on the octahedral sites. As shown in Figure 2d, all the aforementioned three samples take on partially ordered structure. The apparent shoulder bands at 647 and 432 $cm^{-1}$ suggest a higher degree of Ni/Mn ordering for the sample QC. In addition, the shift of absorption band at 593 $cm^{-1}$ to 588 $cm^{-1}$ and the increasing intensity ratio of this band to the absorption band at 623 $cm^{-1}$ ($I_{588}/I_{623}$) further confirmed the higher ordering level for the sample prepared by organic precipitation method.

The electrochemical properties of the organic precipitation method produced sample QC are illustrated in Figure 3. The assembled half-cells were charged at 0.2C and discharged at various rates. The galvanostatic charge curves and discharge curves at various rates are shown in Figure 3a together with sample HC and SS for comparison. Sample QC has a discharge capacity of more than 130 mA h $g^{-1}$ at 0.2C while sample HC and SS take on 124 and 128 mA h $g^{-1}$ separately. Thanks to the favorable intrinsic conductivity of the spinel offered by the three-dimensional lithium ion diffusion path, all the three samples deliver more than 98% reversible capacity of 0.2C when discharged at 1.0C. Apparently, sample QC outperforms the other two samples when discharged at high rate currents. When discharged at 5C, sample QC delivers a specific discharge capacity of 104 mA h $g^{-1}$, which is 80% of its reverse capacity at 0.2C. On the other hand, samples HC and SS deliver 93 and 96 mA h $g^{-1}$ separately at 5C, which is 75% of their reverse capacity at 0.2C. Even at 10C, sample QC still delivers a specific discharge capacity of 75 mA h $g^{-1}$ with a visible plateau at 4.0 V. By contrast, only 42% and 29% of their reverse capacity at 0.2C can be exploited from sample HC and SS, which are 52 and 37 mA h $g^{-1}$, respectively. Moreover, the operation voltage of sample HC drops to about 3.8 V due to severe polarization at high current density. As to sample SS, even no plateau can be observed in its 10C discharge profile.

It should be noted that both samples QC and SS have obvious part capacity in 4 V region, which reflects the redox reaction between the $Mn^{3+}/Mn^{4+}$ couple. This can be further


dx.doi.org/10.1021/am4029526 | ACS Appl. Mater. Interfaces 2013, 5, 10227−10232

detected from the broad peaks at approximately 4.1 V presented in their CV curves as Figure 3c shows. There is a contradiction for the presence of $Mn^{3+}$. On the one hand the energy density decreases with increased amount of $Mn^{3+}$ for its lower redox potential, while on the other hand the presence of $Mn^{3+}$ leads to better rate capability since it has superior electronic conductivity to $Mn^{4+}$. For further analysis, the detail of capacity distribution and energy density were compared in Table 2. When dividing the discharge capacity into two parts

**Table 2. Discharge Capacity and Energy Density of Samples SS, HC, and QC**

| | discharge capacity at 0.2C | | | | | |
|---|---|---|---|---|---|---|
| | 5.0–3.3 V | 5.0–4.2 V | | 4.2–3.3 V | | |
| sample | mA h $g^{-1}$ | mA h $g^{-1}$ | % | mA h $g^{-1}$ | % | energy density/ mW h $g^{-1}$ |
| SS | 127.53 | 111.34 | 87.30 | 16.19 | 12.70 | 581.12 |
| HC | 124.26 | 118.63 | 95.47 | 5.63 | 4.53 | 577.08 |
| QC | 130.76 | 120.23 | 91.95 | 10.53 | 8.05 | 602.19 |

with 4.2 V as the separatrix, 12.70% of the 0.2C discharge capacity is from the 4 V region for sample SS. By contrast, it is no more than 10% for both sample QC and SS. Comprehensively, the organic precipitation method produced sample QC has overwhelming superiority with the highest energy density of more than 600 $mWhg^{-1}$. It can also be seen from the CV curves in Figure 3c that the organic coprecipitation sample QC shows lower anodic peak (delithiation) potential and smaller anodic/cathodic peak potential difference than sample SS, indicating lower polarization and better lithium insertion/extraction reversibility. The cycle performance of organic precipitation method produced sample QC is plotted in Figure 3b. The specific discharge capacity was maintained above 110 mA h $g^{-1}$ after 90 cycles with stable columbic efficiency. Same reversible capacity can be regained when cycled at 0.2C after high rate current cycles indicating steady structure transformation during $Li^+$ extraction/insertion.

To further figure out the structure tolerance and kinetics behavior for $Li^+$ migration, EIS results of sample QC and SS were compared in Figure 4. EIS tests were carried out on fresh cells after charging to 4.5 V and cells at open circuit voltage (OCV) after discharging, separately, in the frequency range of 200 kHz to 5 mHz with an ac amplitude of 5 mV. Normally, the Nyquist spectrum of such cathode process consists of a high-frequency semicircle, which arises from the interfacial layer resistance ($R_s$) and capacitance ($CPE_s$) between electrolyte and solid electrode, a second semicircle at medium-to-low frequency, which is associated with the charge transfer resistance ($R_{ct}$) and double-layer capacitance ($CPE_{dl}$), and a low frequency rising line representing the Warburg impedance ($Z_w$) due to solid-state diffusion of Li ions in the bulk of the intercalation compound.[36−38] Nyquist plots were fitted based on such equivalent circuits as the inset of Figure 4a shows, and the fitting results are listed in Table 3. Cells of both of the

**Table 3. EIS fitting results of sample SS and QC**

| | charged to 4.5 V | | | OCV after discharging | | |
|---|---|---|---|---|---|---|
| sample | $R_e/\Omega$ | $R_s/\Omega$ | $R_{ct}/\Omega$ | $R_e/\Omega$ | $R_s/\Omega$ | $R_{ct}/\Omega$ |
| SS | 3.224 | 96.3 | 25.8 | 3.192 | 117.7 | 943.0 |
| QC | 7.719 | 136.6 | 31.5 | 5.395 | 26.4 | 577.7 |

samples have similar electrolyte resistance ($R_e$) lower than 10 Ω, and the ($R_e$) values remained almost constant no matter at charged or discharged state. This should be owed to the little variation of electrolyte concentration and conductivity.[39] It is interesting that sample SS has lower interfacial layer resistance ($R_s$) and charge transfer resistance ($R_{ct}$) than sample QC on fresh cells, maybe because of the lower specific surface area and the expanded lattice. Interfacial layer resistance ($R_s$) decreased from 136.6 to 26.4 Ω after cycles for sample QC. It is expected that the preferred (111) crystal plane orientation and smooth particle surface favor the formation of solid/electrolyte interphase (SEI) in good condition. Charge transfer resistance ($R_{ct}$) evidently increased after cycles for both sample QC and SS responsible for the capacity fading. Sample QC possesses a much smaller rising (from 31.5 to 577.7 Ω) than sample SS (from 25.8 to 943.0 Ω). On the other hand, double-layer capacitance ($CPE_{dl}$) decreases obviously after being cycled and discharged. For sample SS, $CPE_{dl}$ cut down from 6.52 mF to 19.29 μF. For sample QC, it decreased from 4.91 mF to 11.23 μF. In the cycled case, the medium-to-low frequency semicircle

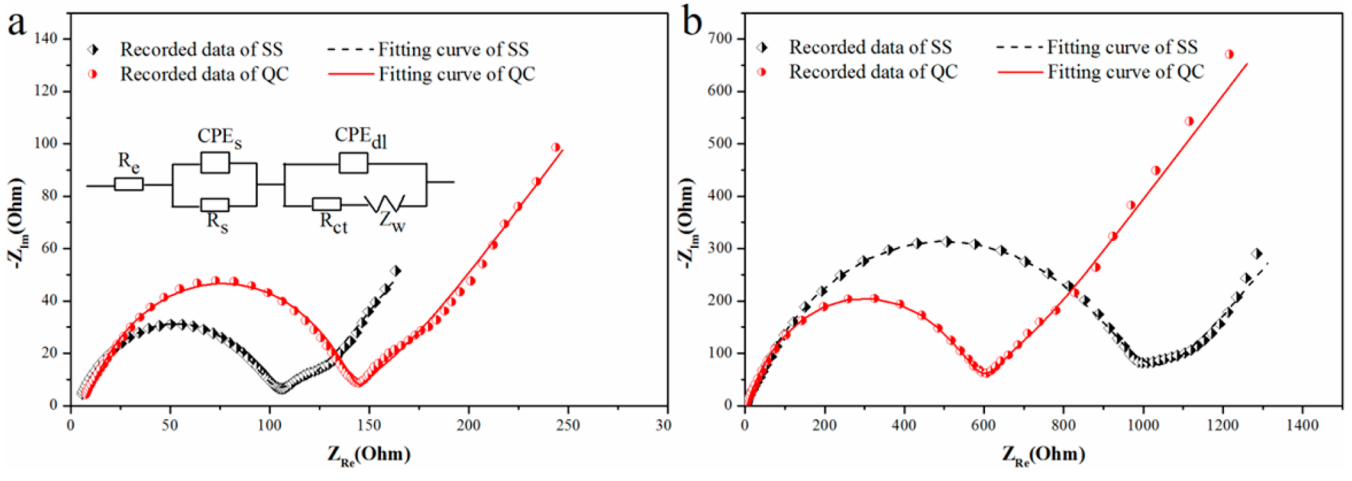


**Figure 4.** Nyquist plots and fitting curves of sample QC and SS performed on (a) fresh cells after charged to 4.5 V and (b) cells at OCV after discharging and equivalent circuit for fitting (inset of a).

is invisible under the extremely discharged conditions; only the high frequency semicircle remains, which is consistent with previous reports.[31,40] According to the fitting results, the $R_s$ and $R_{ct}$ of sample QC are 26.4 and 577.7 Ω, respectively, both of which are much lower than 117.7 and 943.0 Ω, respectively, from sample SS. The lowered interfacial resistance and charge transfer resistance lead to reduced ohmic polarization and activation polarization during repeated lithiation/delithiation, corroborating the aforementioned superior rate capability and structure tolerance of sample QC.

## 4. CONCLUSIONS

A novel organic coprecipitation method has been developed to synthesize spinel $LiNi_{0.5}Mn_{1.5}O_4$. Compared with normal hydroxide coprecipitation method, this route is more convenient. Moreover, the formation of $Li_xNi_{1-x}O$ impurities and oxygen deficient can be greatly restrained. The FTIR spectra indicate its partially ordered structure but a little higher ordering level. EIS fitting results confirmed the lowered interfacial resistance and charge transfer resistance, which is coincident with the superior rate capacity and structure tolerance for lithium migration. This can be explained by the low-extent confusion between lithium ions and transition metal ions as revealed by XRD patterns.

## ■ ASSOCIATED CONTENT

### Ⓢ Supporting Information

Differential capacity vs voltage curves; polarization potential differences of redox reaction at around 4.7 V. This material is available free of charge via the Internet at http://pubs.acs.org.

## ■ AUTHOR INFORMATION


### Corresponding Authors

*E-mail: chm_fengjj@ujn.edu.cn (J.J.F.).
*E-mail: stanwhit@gmail.com (M.S.W.).


### Notes

The authors declare no competing financial interest.

## ■ ACKNOWLEDGMENTS

This work is financial supported by International Cooperation Training Program of excellent teachers in Shandong colleges and universities, Primet Precision Materials Inc., and National Natural Science Foundation of China (51102114)

## ■ REFERENCES


(1) Whittingham, M. S. *Chem. Rev.* **2004**, *104*, 4271−4302.
(2) Goodenough, J. B.; Kim, Y. *Chem. Mater.* **2010**, *22*, 587−603.
(3) Cheng, F.; Liang, J.; Tao, Z.; Chen, J. *Adv. Mater.* **2011**, *23*, 1695−1715.
(4) Kang, K.; Meng, Y. S.; Bréger, J.; Grey, C. P.; Ceder, G. *Science* **2006**, *311*, 977−980.
(5) Tarascon, J. M.; Armand, M. *Nature* **2001**, *414*, 359−367.
(6) Li, G.; Ikuta, H.; Uchida, T.; Wakihara, M. *J. Electrochem. Soc.* **1996**, *143*, 178−182.
(7) Lee, Y. J.; Park, S. H.; Eng, C.; Parise, J. B.; Grey, C. P. *Chem. Mater.* **2002**, *14*, 194−205.
(8) Sakunthala, A.; Reddy, M.V.; Selvasekarapandian, S.; Chowdaria, B.V.R.; Selvin, P. C. *Electrochim. Acta* **2010**, *55*, 4441−4450.
(9) Reddy, M. V.; Raju, M. J. S.; Sharma, N.; Quan, P. Y.; Nowshad, S. H.; Emmanuel, H. E.; Peterson, V. K.; Chowdari, B. V. R. *J. Electrochem. Soc.* **2011**, *158*, A1231−A1236.
(10) Sigala, C.; Guyomard, D.; Verbaere, A.; Piffard, Y.; Tournoux, M. *Solid State Ionics* **1995**, *81*, 167−170.
(11) Amine, K.; Tukamoto, H.; Yasuda, H.; Fujita, Y. *J. Electrochem. Soc.* **1996**, *143*, 1607−1613.
(12) Gao, Y.; Myrtle, K.; Zhang, M.; Reimers, J. N.; Dahn, J. R. *Phys. Rev. B* **1996**, *54*, 16670−16675.
(13) Zhong, Q.; Bonakclarpour, A.; Zhang, M.; Gao, Y.; Dahn, J. R. *J. Electrochem. Soc.* **1997**, *144*, 205−213.
(14) Xu, B.; Qian, D.; Wang, Z.; Meng, Y. S. *Mater. Sci. Eng., R* **2012**, *73*, 51−65.
(15) Reddy, M. V.; Rao, G. V. S.; Chowdari, B. V. R. *Chem. Rev.* **2013**, *113*, 5364−5457.
(16) Masquelier, C.; Croguennec, L. *Chem. Rev.* **2013**, *113*, 6552−6591.
(17) Chen, Z.; Zhu, H.; Ji, S.; Linkov, V.; Zhang, J.; Zhu, W. *J. Power Sources* **2009**, *189*, 507−510.
(18) Sha, O.; Wang, S.; Qiao, Z.; Yuan, W.; Tang, Z.; Xu, Q.; Su, Y. *Mater. Lett.* **2012**, *89*, 251−253.
(19) Reddy, M. V.; Cheng, H. Y.; Tham, J. H.; Yuan, C. Y.; Goh, H. L.; Chowdari, B. V. R. *Electrochim. Acta* **2012**, *62*, 269−275.
(20) Zhang, X.; Cheng, F.; Zhang, K.; Liang, Y.; Yang, S.; Liang, J.; Chen, J. *RSC Adv.* **2012**, *2*, 5669−5675.
(21) Jafta, C. J.; Mathe, M. K.; Manyala, N.; Roos, W. D.; Ozoemena, K. I. *ACS Appl. Mater. Interfaces* **2013**, *5*, 7592−7598.
(22) Feng, J.; Liu, X.; Zhang, X.; Jiang, J.; Zhao, J.; Wang, M. *J. Electrochem. Soc.* **2009**, *156*, A768−A771.
(23) Zhou, L.; Zhao, D.; Lou, X. *Angew. Chem., Int. Ed.* **2012**, *51*, 239−241.
(24) Qian, Y.; Deng, Y.; Shi, Z.; Zhou, Y.; Zhuang, Q.; Chen, G. *Electrochem. Commun.* **2013**, *27*, 92−95.
(25) Xu, G.; Xu, Y.; Fang, J.; Fu, F.; Sun, H.; Huang, L.; Yang, S.; Sun, S. *ACS Appl. Mater. Interfaces* **2013**, *5*, 6316−6323.
(26) Li, Z.; Chernova, N. A.; Feng, J.; Upreti, S.; Omenya, F.; Whittingham, M. S. *J. Electrochem. Soc.* **2012**, *159*, A116−A120.
(27) Larson, A.C.; Von, Dreele, R. B. *Los Alamos Natl. Lab., [Rep.] LA (U.S.)* **2004**, 86−748.
(28) Toby, B. H. *J. Appl. Crystallogr.* **2001**, *34*, 210−213.
(29) Ban, C.; Li, Z.; Wu, Z.; Kirkham, M. J.; Chen, L.; Jung, Y. S.; Payzant, E. A.; Yan, Y.; Whittingham, M. S.; Dillon, A. C. *Adv. Energy Mater.* **2011**, *1*, 58−62.
(30) Hai, B.; Shukla, A. K.; Duncan, H.; Chen, G. *J. Mater. Chem. A* **2013**, *1*, 759−769.
(31) Xiao, J.; Chen, X.; Sushko, P. V.; Sushko, M. L.; Kovarik, L.; Feng, J.; Deng, Z.; Zheng, J.; Graff, G. L.; Nie, Z.; Choi, D.; Liu, J.; Zhang, J.; Whittingham, M. S. *Adv. Mater.* **2012**, *24*, 2109−2116.
(32) Bai, Z.; Fan, N.; Ju, Z.; Sun, C.; Qian, Y. *Mater. Lett.* **2012**, *76*, 124−126.
(33) Lafont, U.; Locati, C.; Borghols, W. J. H.; Łasińska, A.; Dygas, J.; Chadwick, A.V.; Kelder, E. M. *J. Power Sources* **2009**, *189*, 179−184.
(34) Ariyoshi, K.; Iwakoshi, Y.; Nakayama, N.; Ohzuku, T. *J. Electrochem. Soc.* **2004**, *151*, A296−A303.
(35) Kunduraci, M.; Amatucci, G. G. *J. Electrochem. Soc.* **2006**, *153*, A1345−A1352.
(36) Duncan, H.; Lebdeh, Y. A.; Davidson, I. J. *J. Electrochem. Soc.* **2010**, *157*, A528−A535.
(37) Reddy, M. V.; Rao, G. V. S.; Chowdari, B. V. R. *J. Phys. Chem. C* **2007**, *111*, 11712−11720.
(38) Prabu, M.; Reddy, M. V.; Selvasekarapandian, S.; Raa, G. V. S.; Chowdari, B.V.R. *Electrochim. Acta* **2013**, *88*, 745−755.
(39) Zhang, S.S.; Xu, K.; Jow, T. R. *Electrochim. Acta* **2004**, *49*, 1057−1061.
(40) Shaju, K. M.; Bruce, P. G. *Dalton Trans.* **2008**, *37*, 5471−5475.